JOURNAL OF GUIDANCE, CONTROL, AND DYNAMICS
Vol. 32, No. 3, May–June 2009

Missile Autopilot Design: Gain-Scheduling and the Gap Metric

Spilios Theodoulis* and Gilles Duc†
École Supérieure d'Électricité, F91192 Gif-sur-Yvette, France

DOI: 10.2514/1.34756

This paper presents a systematic methodology for the synthesis of global gain-scheduled controllers for nonlinear time-varying systems. A controller of this type is used to compute the pitch-axis autopilot of an air–air missile. The missile model used is considered a benchmark for testing autopilot controllers in the academic and industrial communities. The missile's dynamics are linearized at a small set of operating points for which proportional–integral/proportional-type controllers are designed, to shape the frequency response of the linear plants' dynamics. A new set of operating points is computed afterward using the connection between the gap metric and the $\mathcal{H}_\infty$ loop-shaping theory. Then, reduced-order, static, $\mathcal{H}_\infty$ loop-shaping controllers are designed for this set of points using linear matrix inequality optimization techniques. Finally, the global gain-scheduled controller is obtained by interpolating the proportional–integral/proportional and the loop-shaping controllers' gains over the missile's flight envelope. The simulation results given show the generality and effectiveness of the proposed control strategy in terms of the operating point selection, stability, performance and robustness, of the closed loop.

I. Introduction

ONE of the most important methods of dealing with the control of nonlinear time-varying systems is gain scheduling. This method is often preferred over pure nonlinear ones due mainly to its generality, simplicity, and ease of implementation, although it does not always provide controllers that guarantee closed-loop stability and performance. Its advantages are mainly due to the abandonment of the original nonlinear controller construction problem in favor of a linear controller-based one.

Two main methods for the synthesis of gain-scheduled controllers exist: the linear parameter varying (LPV) based one and the linearization-based one. The LPV-based method synthesizes controllers for the nonlinear plant by reformulating it as a linear time-varying model. This method is extensively studied and gives stability guaranties in the cases in which it succeeds in finding a controller. The linearization-based method uses linear time invariant (LTI) models of the nonlinear plant and can be decomposed into three separate stages [1,2]. First, an appropriate vector of variables (or scheduling vector), ϱ, characterizing the operating domain of the original nonlinear plant is chosen. The operating points of the plant are then parameterized in terms of this vector, and the nonlinear system is linearized at these points. Second, the linear models obtained during the first step are fed to a suitable LTI controller computation machinery (e.g., $\mathcal{H}_2$ or $\mathcal{H}_\infty$ synthesis). The LTI controllers computed stabilize and guarantee the performance of the nonlinear plant at the vicinity of each operating point. Third, a global nonlinear gain-scheduled controller is obtained by blending the LTI controllers according to the scheduling vector that is measured in real time. Various methods exist to blend the LTI controllers, such as state-feedback/observer-gain interpolation, state-space matrix interpolation, controller signal blending, transfer function coefficient interpolation, zero-pole-gain interpolation, or simple controller switching (see [1,2] and the references therein).

The use of gain scheduling for the control of real-world systems is appreciated for different reasons. First, this technique is attractive because accurate mathematical models are unavailable or impractical for such systems and the resulting model uncertainty can be treated by computing the LTI controllers using suitable robust control synthesis techniques. Second, given that the plant's dynamics depend heavily on the scheduling vector (such as altitude and speed for aeronautical systems), an adaptive controller scheme being updated using this vector seems straightforward. Third, from a computation/ implementation point of view, gain scheduling is particularly suited for real-world application due to the controller's easy online computation. Indeed, to calculate the nonlinear control law, there are only two things needed: a collection of LTI controllers, and an interpolation strategy properly parameterized by the scheduling vector. Thus, a gain-scheduling controller needs few resources to be implemented in a real-world system.

Gain-scheduling schemes have been widely applied, particularly on missile autopilot design problems, due to the advantages that they present. LPV-based methods using linear matrix inequality (LMI) formulation are analyzed in [3], whereas those using linearization-based gain scheduling are analyzed in [4,5], with both offering stability guaranties. Ad hoc methods based on the latter method have also been used over the years, each one performing well for the problem that was used [6–13]. Here, a gain-scheduling autopilot for the pitch axis of an air-to-air missile is designed using linearization-based gain scheduling. The contribution to the existing practice is threefold and is connected to the stages of gain-scheduling control already described: synthesis point selection/parameterization, LTI controller computation, and global controller construction by interpolation.

As far as synthesis point selection is concerned, it is clear that a systematic procedure is preferable over an ad hoc one. Indeed, the performance of the final nonlinear controller could be greatly affected by an overgridding (greater computation time) or an undergridding (failure to capture the nonlinear plant's dynamics) of the scheduling vector space. To overcome this problem, the notion of the gap metric and its connection to robust loop-shaping theory is used [14]. A "hands off" algorithm for finding an appropriate gridding for the scheduling vector space is devised using the robustness margin associated to shaped linear plants over the flight envelope.

This systematic procedure dictates a family of operating points for which robust LTI controllers for the shaped LTI plants are computed to increase their robustness margins. The loop-shaping controllers computed are static, output feedback ones, so as to keep a simple

Received 27 September 2007; revision received 2 October 2008; accepted for publication 8 December 2008. Copyright © 2009 by the American Institute of Aeronautics and Astronautics, Inc. All rights reserved. Copies of this paper may be made for personal or internal use, on condition that the copier pay the $10.00 per-copy fee to the Copyright Clearance Center, Inc., 222 Rosewood Drive, Danvers, MA 01923; include the code 0731-5090/09 $10.00 in correspondence with the CCC.

*Doctoral Student, Département Automatique, 3 rue Joliot-Curie. Student Member AIAA.

†Professor, Département Automatique, 3 rue Joliot-Curie.

structure for the control scheme; indeed, this is a major issue for a gain-scheduled controller when it comes to implementation. The general static, output feedback or fixed-order controller design is an open problem; however, LMI-based sufficient conditions can be derived [15] to synthesize suboptimal static $\mathcal{H}_\infty$ output feedback controllers based on the McFarlane and Glover loop-shaping formulation [16].

Finally, as far as interpolation is concerned, a systematic interpolation method is devised to adapt the gain matrices of the controllers throughout all the missile's flight envelope. This method is based on Delaunay triangulation of the scheduling vector space to create interpolation regions automatically, after the synthesis points are selected. Given that the scheduling vector space of the missile is two dimensional, a triangular interpolation is more elegant than the trapezoidal or rectangular one used in most cases.

The paper is organized as follows. In Sec. II, the missile's nonlinear mathematical model is given and the autopilot problem is formulated. In Sec. III, the operating points are parameterized in terms of the scheduling vector and the nominal control is computed. Additional issues concerning the flight envelope are also covered. In Sec. IV, the plant is linearized around a small number of equilibrium points and, after a brief review of classical loop-shaping theory, the initial proportional–integral/proportional (PI/P) shaping filters are designed. Then, the gap metric notion is used to calculate the final synthesis points on the flight envelope via an iterative algorithm and, finally, static $\mathcal{H}_\infty$ loop-shaping controllers are designed for these points. In Sec. V, the structure of the global nonlinear gain-scheduling controller is discussed, whereas, in Sec. VI, extensive simulation results of the proposed control scheme are given.

II. Autopilot Problem Formulation

A. Missile Mathematical Model

The mathematical model of the missile used here [6] describes the dynamics of a highly maneuverable air-to-air missile around its pitch axis, where its state vector x is the angle of attack (AOA) α and its pitch rate is q. The task for the autopilot is to make sure the missile's vertical acceleration, η, tracks varying amplitude reference signals, η_r, using the missile's rudder deflection angle, δ. (From now on the subscripts c, r, f, and δ will denote the commanded, reference, filtered, and difference variables, respectively.) The rudder is in turn controlled by an actuator, and δ follows rudder angle commands, δ_c, provided by the autopilot. The measured variables are the missile's vertical acceleration and pitch rate as well as its Mach number. Finally, the model is valid for $1.5 \le M \le 3$ and -20 deg $\le \alpha \le 20$ deg; α and M thus form the missile's flight envelope. The state dynamics are given by

$$\dot{\alpha}(t) = K_\alpha M(t) C_\alpha[\alpha(t), M(t), \delta(t)] \cos\alpha(t) + q(t) \tag{1}$$

$$\dot{q}(t) = K_{\mathrm{pr}} M^2(t) C_{\mathrm{pr}}[\alpha(t), M(t), \delta(t)] \tag{2}$$

whereas the output dynamics are given by

$$\eta(t) = K_\eta M^2(t) C_\alpha[\alpha(t), M(t), \delta(t)] \tag{3}$$

The functions C_α and C_{pr} are either available from aerodynamic data tables or as polynomial functions of the AOA, tail deflection angle, and Mach number (explicit dependence on time for the functions or variables will be dropped when necessary for the sake of simplicity):

$$C_\alpha[\alpha, M, \delta] = C^*_\alpha[\alpha, M] + d_n((180/\pi)\delta) \tag{4}$$

$$C_{\mathrm{pr}}[\alpha, M, \delta] = C^*_{\mathrm{pr}}[\alpha, M] + d_m((180/\pi)\delta) \tag{5}$$

with

$$C^*_\alpha[\alpha, M] = \mathrm{sgn}(\alpha)\left[a_n\left|\frac{180}{\pi}\alpha\right|^3 + b_n\left|\frac{180}{\pi}\alpha\right|^2 + c_n\left(2 - \frac{M}{3}\right)\left|\frac{180}{\pi}\alpha\right|\right] \tag{6}$$

$$C^*_{\mathrm{pr}}[\alpha, M] = \mathrm{sgn}(\alpha)\left[a_m\left|\frac{180}{\pi}\alpha\right|^3 + b_m\left|\frac{180}{\pi}\alpha\right|^2 + c_m\left(-7 + \frac{8M}{3}\right)\left|\frac{180}{\pi}\alpha\right|\right] \tag{7}$$

The actuator dynamics are modeled as follows:

$$\ddot{\delta}(t) + 2\zeta\omega_a\dot{\delta}(t) + \omega_a^2\delta(t) = \omega_a^2\delta_c(t) \tag{8}$$

Finally, the Mach dynamics are given as follows:

$$\dot{M}(t) = \frac{1}{\upsilon_s}[-|\eta(t)|\sin|\alpha(t)| + A_x M^2(t)\cos\alpha(t)], \qquad M(0) = M_0 \tag{9}$$

The various constants appearing in Eqs. (1–9) are shown in Table 1.

B. Autopilot Performance and Robustness Specifications

The autopilot specifications are given in terms of performance and robustness. There are two performance goals to be achieved: good tracking characteristics (P1), and small missile rudder deflection rates (P2). There are also two goals for robustness: robust stability under aerodynamic coefficient variation (R1), and high-frequency open-loop gain attenuation for the autopilot to avoid exciting unmodeled structural dynamics (R2). The specifications are taken from [6]:

P1: Track step commands in η_r of various amplitudes with a time constant of $\tau \le 0.35$ s and overshoot $M_p \le 10\%$ and steady-state error $e_{\mathrm{ss}} \le 1\%$.

P2: The maximum deflection rate, $\dot{\delta}_{\max}$, of the missile's rudder angle should not exceed 25 deg/s for $1g$ step commands of η_r for the missile's flight envelope.

R1: The missile should exhibit robust stability for all its flight envelope with the coefficients (a_m, b_m, and c_m) and d_m varying independently around their nominal values by 25%.

R2: The linearized system should maintain at least a 30 dB attenuation at 300 rad/s for the gain amplitude of the obtained transfer function when the loop is opened just before the actuator.

III. Flight Envelope Parametrization

A. Nominal Control

The global nonlinear control law providing the rudder command angle, δ_c, consists of two separate signals: the nominal control signal, δ_r, and the closed loop error signal, δ_δ. Their combined action ensures correct tracking of the reference signal, η_r (see Fig. 8).

The nominal control signal, δ_r, depends on the output, Mach number, and AOA and can be computed from Eq. (3):

Table 1 Missile model coefficients

Constant	Value	Unit[a]
K_α	0.0206898	s^{-1}
K_{pr}	1.2319409	s^{-2}
K_η	0.6662393	
a_n	0.000103	deg^{-3}
b_n	−0.00945	deg^{-2}
c_n	−0.1696	deg^{-1}
d_n	−0.034	deg^{-1}
a_m	0.000215	deg^{-3}
b_m	−0.0195	deg^{-2}
c_m	0.051	deg^{-1}
d_m	−0.206	deg^{-1}
ζ	0.7	
ω_a	150.0	rad/s
υ_s	315.89472	m/s
A_x	−1.9607424	

[a]The constants are from [6] and are converted to SI units.

$$\delta_r(\eta_r, M, \alpha) = \frac{\frac{\eta_r}{K_\eta M^2} - C^*_\alpha(\alpha, M)}{d_n(\frac{180}{\pi})} \tag{10}$$

supposing that the system operates around an equilibrium-reference point ($\dot{q}_r = 0$).

The Mach number, considered as a variable and not as a state, varies slowly during reference point operation, making δ_r time dependent. From the following analysis, it will be demonstrated that the state corresponding to a given η_r is also time varying due to Mach variation. The nominal control, δ_r, as a function of α, cannot be computed directly from Eq. (10) because α is unavailable for feedback. Thus, it must be computed only as a function of known quantities, namely, the scheduling vector $\varrho = [\,\eta_r \quad M\,]$.

Given that the Mach number varies slowly, an equilibrium state could be assigned for any constant output reference value η_r and, as a result, the left-hand sides of Eqs. (1) and (2) go to zero. Replacing the expression for $\delta_r(\eta_r, M, \alpha)$ from Eq. (10) into Eq. (2), the following equation for α is obtained as a function of the scheduling vector components:

$$C^*_{\mathrm{pr}}(\alpha, M) - \frac{d_m}{d_n} C^*_\alpha(\alpha, M) + \frac{1}{K_\eta}\frac{d_m}{d_n}\frac{\eta_r}{M^2} = 0 \tag{11}$$

Equation (11) is polynomial of the third order in α and can be solved explicitly by the classic method of Cardano. For both positive and negative values of η_r, the solutions are symmetrical and only one of the three has a physical sense. Having obtained α as a function of the scheduling vector ϱ, the nominal control $\delta_r(\eta_r, M)$ can be computed from Eq. (10) (see Fig. 1). Finally, the corresponding value $q(\eta_r, M)$ is found by substituting Eqs. (10) and (11) into Eq. (1) and supposing that $\dot{\alpha} = 0$.

B. Flight Envelope

In Sec. III.A, the nominal control $\delta_r(\varrho)$ is computed without considering any limitations on α, thus resulting in a rectangular flight envelope (see Fig. 2). However, limitations on α do exist (-20 deg $\leq \alpha \leq 20$ deg) and must be translated into limits on η by solving Eq. (11) for η_r considering the extremal values $\alpha = \pm 20$ deg for every $1.5 \leq M \leq 3$, thus resulting in an admissible η-parameterized flight envelope of nonconvex trapezoidal form (see Fig. 2).

In Fig. 2, this η-parameterized envelope is shown (white trapezoidal symmetric regions) along with two approximations; the aforementioned rectangular and a convex trapezoidal. The two shaded regions together represent the total redundant surface if the first approximation is used, as in most works. The small darker shaded region alone (finally retained) shows the redundant surface if the second convex approximation is considered.

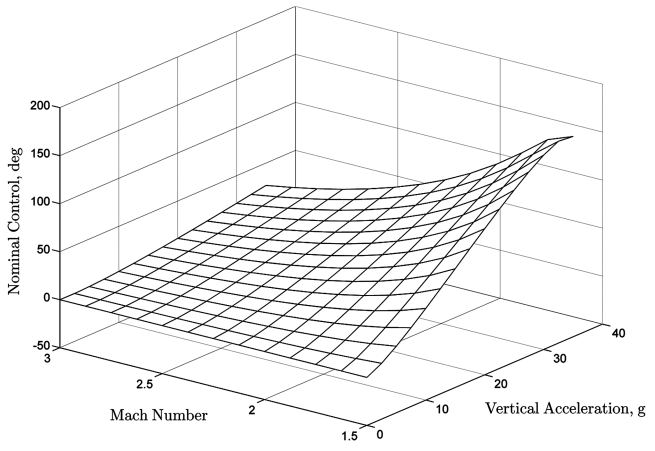

Fig. 1 Nominal control surface.

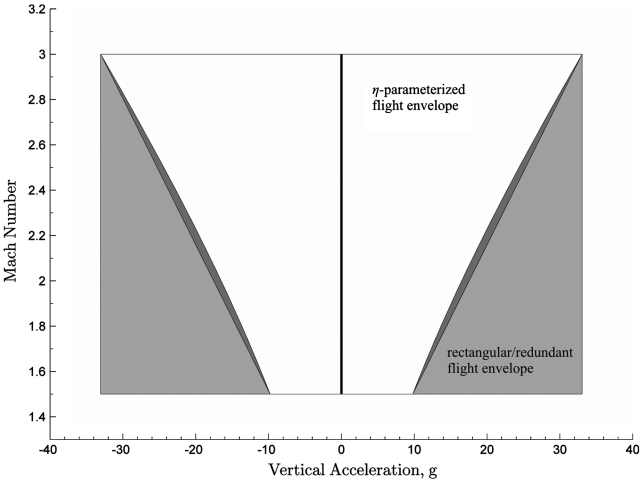

Fig. 2 Missile flight envelope.

IV. Linear Time Invariant Controller Synthesis

A nonlinear gain-scheduling controller is, in general, computed using linear controllers computed around a number of operating points of the nonlinear system (see [1,2] for more details on linearization-based gain scheduling). In Sec. IV.A, the procedure of obtaining these linear models is described for any chosen operating points. In Secs. IV.B–IV.D, the procedure of computing linear controllers is detailed, whereas, finally in Sec. IV.E, the algorithm used to choose these operating points is presented.

A. Model Linearization

The missile's equilibrium operating points have been parameterized in Sec. III.A, whereas its flight envelope has been obtained in Sec. III.B by means of the scheduling vector ϱ. Now, LTI models of the missile's nonlinear model will be calculated for every candidate operating point inside the flight envelope.

For any reference value of the scheduling vector ϱ_r, an output-parameterized LTI model of the missile is computed as in Eqs. (12) and (13), with $f\colon \mathbb{R}^2 \to \mathbb{R}^2$, $h\colon \mathbb{R}^2 \to \mathbb{R}$ being the nonlinear functions of the state and the output (right-hand sides of Eqs. (1–3), respectively):

$$\dot{x_\delta} = \nabla_x f(\varrho_r) x_\delta + \nabla_\delta f(\varrho_r)\delta_\delta \tag{12}$$

$$\eta_\delta = \nabla_x h(\varrho_r) x_\delta + \nabla_\delta h(\varrho_r)\delta_\delta \tag{13}$$

The difference quantities x_δ, δ_δ, and η_δ are defined as

$$x_\delta = x - x(\varrho_r) \tag{14}$$

$$\delta_\delta = \delta - \delta(\varrho_r) \tag{15}$$

$$\eta_\delta = \eta - \eta_r \tag{16}$$

After calculating the derivatives in Eqs. (12) and (13), the following matrices are obtained (the pitch rate q being also an output):

$$A(\varrho_r) = \nabla_x f(\varrho_r) = \begin{pmatrix} A_{11}(\varrho_r) & 1 \\ A_{21}(\varrho_r) & 0 \end{pmatrix} \tag{17}$$

$$B(\varrho_r) = \nabla_\delta f(\varrho_r) = \begin{pmatrix} B_{11}(\varrho_r) \\ B_{21}(\varrho_r) \end{pmatrix} \tag{18}$$

$$C(\varrho_r) = \begin{pmatrix} \nabla_x h(\varrho_r) & 0 \\ 0 & 1 \end{pmatrix} = \begin{pmatrix} C_{11}(\varrho_r) & 0 \\ 0 & 1 \end{pmatrix} \tag{19}$$

$$D(\varrho_r) = \begin{pmatrix} \nabla_\delta h(\varrho_r) \\ 0 \end{pmatrix} = \begin{pmatrix} D_{11}(\varrho_r) \\ 0 \end{pmatrix} \tag{20}$$

The evolution of the matrix elements in Eqs. (17–20) as a function of the scheduling vector ϱ is demonstrated in Fig. 3; it can be observed that the evolution is smooth enough to justify a gain-scheduling control procedure.

The transfer function G_η (from δ_δ to η_δ) has unstable dynamics for high and low values of M and η_r, respectively, and stable but badly damped dynamics with nonminimum phase zeros for the rest of the flight envelope. The transfer function G_q (from δ_δ to q_δ) has similar dynamics without the nonminimum phase zeros.

B. Loop-Shaping Design Procedure

The method used in this paper to compute linear controllers for use by the gain-scheduled controller is based heavily on the loop-shaping procedure of McFarlane and Glover that appears in [16–18].

For a shaped LTI system G_s, a robust, output feedback, dynamic $\mathcal{H}_\infty$ controller K_∞ can stabilize the plant and, in addition, maximize the closed-loop robustness margin $\epsilon_{\max}$ associated with norm-bounded additive uncertainties on the system's left normalized coprime factors (NCFs). This control strategy has proven to be very effective and can be decomposed into three distinct steps.

Step 1: Loop-Shaping. The initial open loop system transfer function G (here it is $G = [G_\eta \quad G_q]^T$) is augmented by appropriate pre/postfilters W_1 and W_2 to achieve the performance (and maybe some stability) requirements, shaping the open-loop singular values of G. This can be done using a variety of control synthesis techniques, leading to a shaped-augmented plant $G_s = W_2 G W_1$ (see Fig. 4).

Step 2: Robustness Verification. The associated robustness margin $\epsilon_{\max}$ achieved using G_s from the previous step is calculated. If $\epsilon_{\max} \ll 1$, then the shaping procedure was not successful and the filters W_1 and W_2 should be readjusted. Note that, for the NCF case, the margin $\epsilon_{\max}$ is calculated directly via the Hankel norm of the coprime factor decomposition of G_s in a noniterative manner. As a result, there is no need to calculate the $\mathcal{H}_\infty$ controller K_∞ before deciding on the final W_1 and W_2.

Step 3: Controller Computation and Implementation. For $\epsilon \lesssim \epsilon_{\max}$, calculate a suboptimal $\mathcal{H}_\infty$ controller K_∞ that robustly stabilizes G_s in the face of norm-bounded, additive, left NCF uncertainties, with a stability margin ϵ. Implement the final controller K_s as the series interconnection of the prefilter W_1, the robust controller K_∞, and the postfilter W_2, that is, $K_s = W_1 K_\infty W_2$ (see Fig. 4).

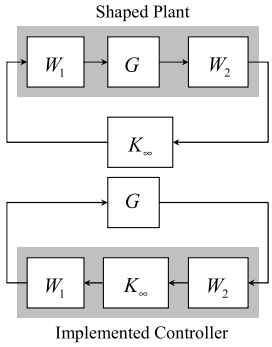

Fig. 4 Loop-shaping procedure block diagram.

For the sake of simplicity, the filters W_1 and W_2 are computed only at a small number of prechosen operating points, whereas an interpolation is used for any other operating point. These controllers, corresponding to steps 1 and 2, are computed in Sec. IV.C.

The $\mathcal{H}_\infty$ controllers of step 3 are presented in Sec. IV.D. In the classical procedure of McFarlane and Glover [16], the resulting dynamic loop-shaping controllers K_s are of an order greater than the plant G. This is a major drawback, especially for gain-scheduling control schemes, because such controllers are difficult to implement. To overcome this inconvenience, *static* $\mathcal{H}_\infty$ output feedback controllers are considered in their place, following [15].

C. Proportional–Integral/Proportional Controller Computation

In this section, the shaping filters W_1 and W_2 of step 1 from Sec. IV.B are computed for any linearized model G of the missile. As mentioned earlier, the open-loop frequency response of the missile must be shaped, for any chosen point inside the flight envelope, to compute the $\mathcal{H}_\infty$ controllers of Sec. IV.D. This frequency shaping is done using PI/P-type controllers in order for W_2 to exhibit the minimal level of complexity.

An inner-loop P controller K_q is first added using pitch rate measurements, and a PI controller, $G_{\text{PI}} = K_p + (K_i/s)$, is then used to regulate the tracking error, forming an outer-loop as in Fig. 5. These two controllers form W_2, whereas W_1 is formed using only the actuator's transfer function G_a.

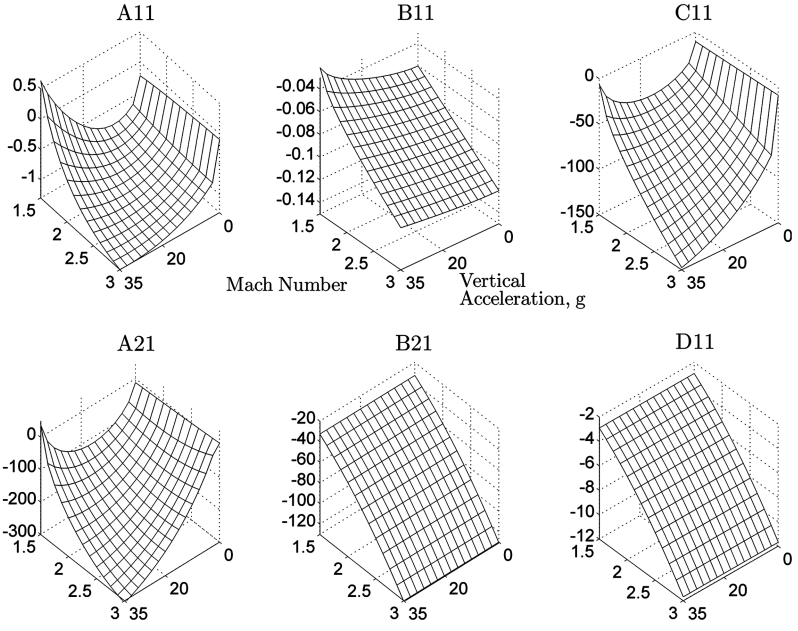

Fig. 3 Matrices of the LTI models.

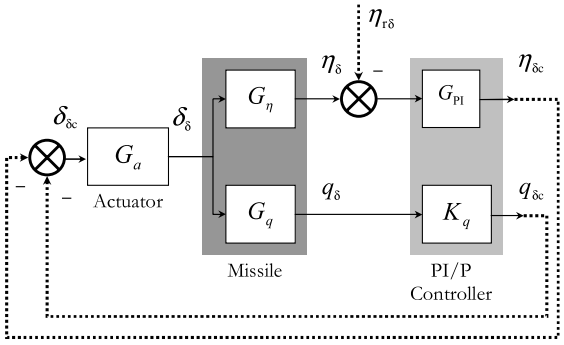

Fig. 5 PI/P controller synthesis block diagram.

To compute the gains K_q, K_p, and K_i of W_2 at every synthesis point, the Simulink® Control Design coupled with the Simulink® Response Optimization toolboxes of MATLAB® are used. Time constraints on the output's step response are imposed in terms of response time, time constant, maximum overshoot/undershoot, and steady-state error. The nine operating points used and the corresponding gains are shown in Table 2 and the gain surfaces in Fig. 6. For the rest of the flight envelope, the gains forming W_2 are obtained using trapezoidal interpolation of the gain triplets computed initially. In this way, the shaping filters are not the optimal choice for any other operating point, but complexity is reduced.

D. Static Loop-Shaping Controller Computation

As remarked in Sec. IV.B, a dynamic loop-shaping controller is not desirable because it is more difficult to interpolate and/or to implement. Because of this fact, a *static* controller is used; however, the corresponding synthesis problem is nonconvex and, thus, difficult to solve. Iterative methods to either render the problem convex (though not guaranteeing a global solution) or methods based on sufficient conditions (though making the problem conservative) can be used. Here, a recently investigated method appearing in [15] is applied, leading to a static controller $K_\infty \in \mathbb{R}^{2\times 1}$.

Consider the already-shaped plant $G_s = \begin{pmatrix} A & B \\ C & D \end{pmatrix}$ with $A \in \mathbb{R}^{n\times n}$, $B \in \mathbb{R}^{n\times m}$, $C \in \mathbb{R}^{p\times n}$, and $D \in \mathbb{R}^{p\times m}$, its minimal left NCF $\begin{bmatrix} \tilde{N} & \tilde{M} \end{bmatrix} = \begin{pmatrix} A+LC & B+LD & L \\ E^{-1/2}C & E^{-1/2}D & E^{-1/2} \end{pmatrix}$, and the generalized plant corresponding to the McFarlane and Glover loop-shaping procedure,

$$P = \begin{pmatrix} A & -LE^{1/2} & B \\ 0 & 0 & I \\ C & E^{1/2} & D \\ C & E^{1/2} & D \end{pmatrix} \tag{21}$$

The matrices in P are defined as $E = I + DD^T$, $L = -(BD^T + ZC^T)E^{-1}$, and $F = I + D^TD$, with $Z = Z^T \geq 0$ being the unique stabilizing solution of the following algebraic Riccati equation:

Table 2 PI/P controller gains per synthesis point

Point	$[\eta_r, M]$	K_p	K_i	K_q
P_1	[0,1.5]	0.1217	0.2683	−0.351
P_2	[4.79,1.5]	0.09	0.6614	−0.464
P_3	[9.59,1.5]	0.077	0.7742	−0.4846
P_4	[0,2.25]	0.0373	0.0596	−0.1791
P_5	[10.48,2.25]	0.0208	0.2782	−0.2394
P_6	[20.97,2.25]	0.0156	0.3221	−0.2524
P_7	[0,3]	0.0322	0.0014	−0.21
P_8	[16.17,3]	0.0068	0.1311	−0.1392
P_9	[32.35,3]	0.0041	0.1602	−0.1516

$$(A - BF^{-1}D^TC)Z + Z(A - BF^{-1}D^TC)^T - ZC^TE^{-1}CZ + BF^{-1}B^T = 0 \tag{22}$$

The following theorem [15] gives sufficient conditions for the existence of robust stabilizing static $\mathcal{H}_\infty$ output feedback controllers for the shaped plant G_s and also ensures

$$\left\| \begin{bmatrix} K_\infty \\ I \end{bmatrix} (I + G_sK_\infty)^{-1}\tilde{M}^{-1} \right\|_\infty < \gamma \tag{23}$$

Theorem 1. Let $L = -(BD^T + ZC^T)E^{-1}$, where $Z = Z^T \geq 0$ is the solution to the aforementioned ARE [Eq. (22)]. There exists a stabilizing static controller K_∞ as in Eq. (23), if $\gamma = \epsilon^{-1} > 1$ and if there exists $R = R^T > 0$ satisfying the following LMIs:

$$(A + LC)R + R(A + LC)^T < 0 \tag{24}$$

$$\begin{pmatrix} AR + RA^T - \gamma BB^T & RC^T - \gamma BD^T & -LE^{1/2} \\ CR - \gamma DB^T & -\gamma E & E^{1/2} \\ -E^{1/2}L^T & E^{1/2} & -\gamma I_p \end{pmatrix} < 0 \tag{25}$$

It should be remarked that Eq. (24) gives a sufficient condition for the existence of the static controller K. This is done by omitting a nonlinear term, $-\gamma RC^TE^{-1}CR$, and, thus, convexifying the synthesis problem. As a result, Eqs. (24) and (25), form a system of LMIs in γ and R and a static controller may be computed after the verification of these feasibility conditions. These inequalities must be optimized for γ attaining a $\gamma > \gamma_{\min}$ always.

Given that $\epsilon_{\max} = 1/\gamma_{\min}$ may be computed before the controller is actually constructed (see step 2 from the loop-shaping procedure of Sec. IV.B), the actual γ obtained from the optimization procedure and $\gamma_{\min}$ can be compared.

Finally, using the bounded real lemma (and after the feasibility constraints are met), the final static controller K_∞ (step 3 from Sec. IV.B) may be calculated as

$$K_\infty = -\tilde{K}(I + D\tilde{K})^{-1} \tag{26}$$

where $\tilde{K}$ is obtained by solving the following LMI:

$$\tilde{A} + \tilde{B}\,\tilde{K}\,\tilde{C} + (\tilde{B}\,\tilde{K}\,\tilde{C})^T < 0 \tag{27}$$

with $\tilde{A}$, $\tilde{B}$, and $\tilde{C}$ being given by

$$\tilde{A} = \begin{pmatrix} AR + RA^T & 0 & RC^T & -LE^{1/2} \\ 0 & -\gamma I_m & 0 & 0 \\ CR & 0 & -\gamma I_p & E^{1/2} \\ -E^{1/2}L^T & 0 & E^{1/2} & -\gamma I_p \end{pmatrix} \tag{28}$$

$$\tilde{B} = \begin{pmatrix} B \\ I_m \\ D \\ 0 \end{pmatrix} \tag{29}$$

$$\tilde{C} = \begin{pmatrix} CR & 0 & 0 & E^{1/2} \end{pmatrix} \tag{30}$$

E. Operating Point Choice Using the Gap Metric

In this section, the connection between the robust stabilization procedure of Sec. IV.B and the gap metric is reviewed, permitting us to devise an algorithm to calculate the static controller synthesis points.

The gap metric in the control literature is due to Zames and El-Sakkary [14], and the connection between robustness optimization under NCF uncertainties and robustness optimization under the gap metric is due to Georgiou and Smith [19].

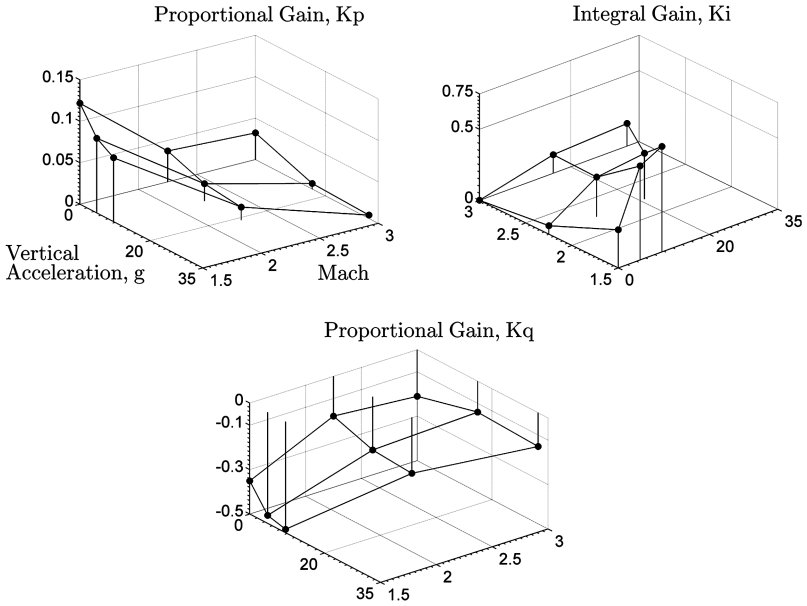

Fig. 6 PI/P controller gain surfaces.

The gap metric δ_g is defined as the distance between the graphs of two LTI systems, G and G_Δ. Its computation is easily done by solving two standard double block $\mathcal{H}_\infty$ problems, resulting in $0 \leq \delta_g(G, G_\Delta) \leq 1$ always. In addition, the gap metric is a measure of how much plant uncertainty a feedback controller can tolerate. The following theorem [19] gives necessary and sufficient conditions for the gap between G and G_Δ on the one hand and, on the other hand, the extent that a controller K_∞ stabilizes a right coprime factor perturbed plant G_Δ, given that it robustly stabilizes a nominal plant G.

Theorem 2. Consider a nominal plant G with a right NCF $G = NM^{-1}$ and a controller K_∞ that robustly stabilizes it. Take a number ϵ with $0 < \epsilon \leq 1$. Then the following two statements are equivalent:

1) The pair $[G_\Delta, K_\infty]$ is stable for all G_Δ with $G_\Delta = (N + \Delta_N)(M + \Delta_M)^{-1}$, where $\Delta_M, \Delta_N \in \mathbb{R}\mathcal{H}_\infty$ and

$$\left\| \begin{pmatrix} \Delta_M \\ \Delta_N \end{pmatrix} \right\|_\infty < \epsilon$$

2) The pair $[G_\Delta, K_\infty]$ is stable for all G_Δ with $\delta_g(G, G_\Delta) < \epsilon$.

Because of Theorems 1 and 2, an algorithm for the choice of controller synthesis points may be devised using the gap metric, keeping always in mind that an optimal controller for coprime factor perturbations is optimal for both left and right factorizations, even though the two types of uncertainty generate different classes of perturbed plants [19]. The latter fact is pointed out because, in Theorem 1, the robust static $\mathcal{H}_\infty$ controllers K_∞ are computed for *left* NCFs of the plant, whereas, in Theorem 2, the connection between these controllers and the gap metric is in terms of *right* NCFs. The algorithm proceeds as follows:

Step 1: Initialization. Choose an equidistant gridding over the one dimension of the flight envelope. Here the Mach number is used because the gap does not vary significantly over M; thus, a set of values $\mathcal{S}_M = [M_1, M_2, \ldots, M_k]$ is obtained. Then take as an initial operating point P_j the one corresponding to $\eta = 0$ and $M = M_1$.

Step 2: Loop Shaping. For the point chosen, a linear model of the plant G_j is obtained using Eqs. (12–20). The model is augmented by the actuator and the PI/P controllers (Fig. 5); thus, the shaped plant $G_{s,j}$ is calculated. The gains of the PI/P controllers are taken as linear interpolations over four scheduling regions (Fig. 6), according to the location of the synthesis point. For the shaped plant $G_{s,j}$, a static $\mathcal{H}_\infty$ output feedback, $\mathcal{H}_\infty$ controller $K_{\infty j}$ is computed using Theorem 1 and the corresponding robustness margin $\epsilon_j = \gamma_j^{-1}$ is obtained from the LMI optimization procedure.

Step 3: Line Search or Reset. Performing a line search for constant M and for increasing values of η_r and applying the same procedure as for the initial point P_j, successive shaped plants $G_{s,f}$ are computed until the gap $\delta_g(G_{s,j}, G_{s,f})$ between the initial shaped plant $G_{s,j}$ and a successive one $G_{s,f}$ is less than or equal to the robustness margin ϵ_j of the initial plant in step 2. If this is the case, a new operating point is chosen and the algorithm jumps to step 2 except for the case in which the end of the flight envelope is reached. In this case, even if $\delta_g(G_{s,j}, G_{s,f}) < \epsilon_j$, the point is selected and the procedure is restarted using the next value of M (this is done for all $M \in \mathcal{S}_M$).

A set of synthesis points is thus obtained following a systematic procedure and avoiding ad hoc rectangular gridding of the flight envelope. A set of static controllers is also obtained for the corresponding operating points, increasing in this way the robustness margins of the plant. In Fig. 7, the γ attained as well as the elements of the static $\mathcal{H}_\infty$ controller gain matrices K_∞ for all computed operating points are shown for a three element set $\mathcal{S}_M$.

V. Nonlinear Controller Construction

A. Controller Form

The global nonlinear gain-scheduled controller is detailed in this section. A controller of this form is used to cover the whole flight envelope of the missile by properly updating the gains K_P, K_q, K_i, and $K_\infty = [K_1 \quad K_2]$, according to the scheduling vector ϱ. In addition, two feedforward controllers, $G_r = K/(s + K_r)$ and $G_{\text{con}} = K_{\text{con}}/(s + K_{\text{con}})$, are used to smooth the reference signal and the gains of the controllers when changing reference points. The time constants of these controllers may be fine-tuned by simulations and are comparable to the time constant of the performance required (see Sec. VI.A for details).

Before giving the form of the gain-scheduled controller (the feedforward action is not taken into account in the equations for the sake of simplicity), two important requirements are noted, following the analysis in [1,2]:

1) The output of the gain-scheduled controller should eliminate the error between the output and the reference, thus providing appropriate steady-state control inputs to the plant for each frozen value of the reference signal. This is ensured by the combined action of the nominal control and the integral effort of the PI controller.

2) The linearization of the gain-scheduled controller at the synthesis points should match the linear controllers designed to ensure valid local stability and performance requirements for the linear plants.

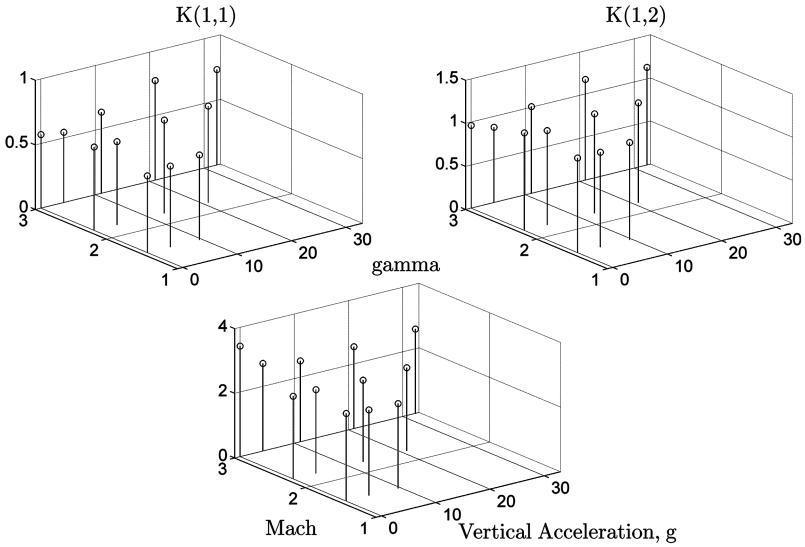

Fig. 7 Performance level and static controller gains.

A possible but not unique realization of this global gain-scheduled controller (Fig. 8) is ($x = [\alpha \quad q]^T$, $\dot{x}_c = \eta_\delta$, $u = \delta$, $y = [\eta \quad q]^T$),

$$\dot{x}_c = A_c(\varrho)(x_c - x_{c,r}(\varrho)) + B_c(\varrho)(y - y_r(\varrho)) \tag{31}$$

$$u = C_c(\varrho)(x_c - x_{c,r}(\varrho)) + D_c(\varrho)(y - y_r(\varrho)) + u_r(\varrho) \tag{32}$$

The controller matrices are given by

$$A_c(\varrho) = 0 \tag{33}$$

.

$$B_c(\varrho) = [1 \quad 0] \tag{34}$$

$$C_c(\varrho) = K_1(\varrho)K_i(\varrho) \tag{35}$$

$$D_c(\varrho) = [K_1(\varrho)K_p(\varrho) \quad K_2(\varrho)K_q(\varrho)] \tag{36}$$

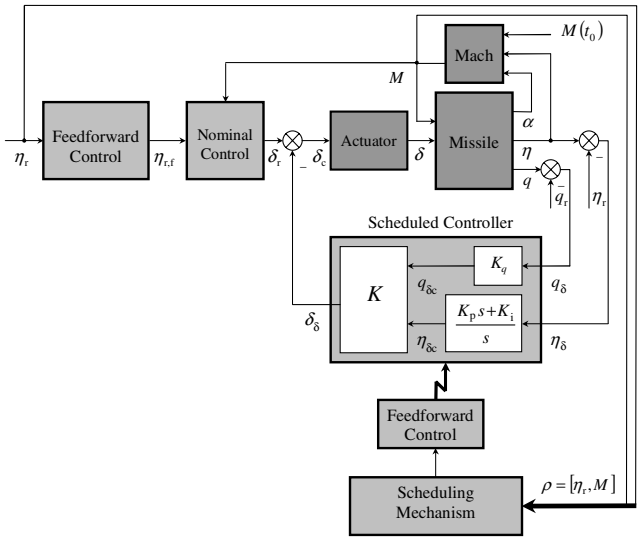

Fig. 8 Global gain-scheduled controller.

B. Controller Gain Interpolation

The scheduling mechanism permitting the interpolation of the gains of the PI/P and the loop-shaping controller, thus covering the flight envelope of the missile, is detailed in this section.

The gains of the PI/P controllers are scheduled using the nine synthesis points (see Fig. 6) that form four trapezoidal interpolation regions. All three time-varying gains are scheduled according to the evolution of the scheduling vector and by using the corners of the corresponding trapezoid (where the corners are numbered by indices 1, 2, 3, and 4 in a counterclockwise manner, starting from the lower left corner).

Given a reference trajectory point P, find the coordinates P_{14} of the point being the projection of P onto the side d_{14} of the trapezoid. Then, find a linear interpolation for the gains using the controllers of the corners 1 and 4. Obtain also the gains on the symmetrical projection of point P onto the side d_{23} of the trapezoid (point P_{23}) using the controllers of the corners 2 and 3. Finally, perform a linear interpolation between the gains at points P_{14} and P_{23} to obtain the final interpolated gains at point P.

The gains of the static $\mathcal{H}_\infty$ controller are scheduled using the family of synthesis points obtained after applying the gap metric selection algorithm (Sec. IV.E). The flight envelope is divided into a number of horizontal bands equal to the number of intervals of $\mathcal{S}_M$ (see Fig. 9). As the reference trajectory moves onto the flight envelope, it passes from one band to another. Each band is triangulated using Delaunay triangulation of the synthesis points, and the gains are interpolated using the triangle that contains the

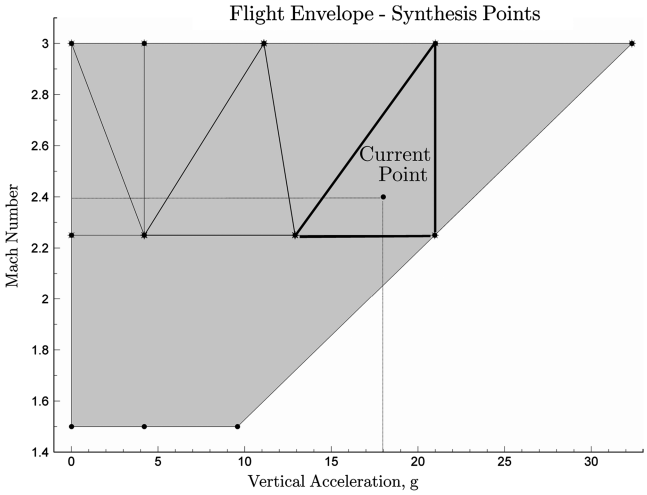

Fig. 9 Triangulation of the flight envelope.

current reference point. To perform the triangular interpolation, the plane defined by the gains of each triangle corner is used to compute the value of each gain for any point in the triangle.

VI. Simulation Results

A. Trimming and Linear Analysis

In this section, feedforward gain trimming and linear simulation results are presented.

Before performing the nonlinear simulations of the next sections, the gains K_r and K_{con} of the feedforward controllers (applied on the reference trajectory and on the interpolated gains) detailed in Sec. V.A should be selected. Two sets, $\mathcal{S}_r = [4, 4.1, \ldots, 5]$ and $\mathcal{S}_{\text{con}} = [7, 7.25, \ldots, 9]$, of values for the gains are defined, and the nonlinear controller is simulated for a $30g$ reference step. To decide on the choice for the gains, the rise and settling times as a function of the overshoot and the minimum as a function of the maximum percentages of the output's deviation with respect to the reference signal are plotted (see Fig. 10).

From the figures it can be seen that, for each one of the 11 families of points (each one corresponding to a constant value of K_r), the rise and settling times get smaller whereas the overshoot gets bigger. Meanwhile the minimum and maximum deviations get bigger. By inspecting the step response in Fig. 10, a good tradeoff between all these constraints is achieved for $K_r = 4.4$ and $K_{\text{con}} = 8.25$ (thick black line). These values are used from now on for the following sections.

To investigate the plant's robustness with the PI/P and the loop-shaping controllers, the plant is linearized at 200 random points inside its flight envelope. (The pseudorandom number generator used here and in the following sections uses a Gaussian distribution with zero mean and unitary standard deviation; the results are scaled afterward to produce numbers with an appropriate standard deviation.) The appropriate gains are computed by interpolation and the open-loop transfer function from the input of the actuator to the output of the loop-shaping controller is obtained. The robustness margins are shown on a Nichols chart (see Fig. 11); it can be observed that the minimum gain/phase margins are 10.5 dB and 51 deg, respectively.

B. Nonlinear Simulations: Nominal Case

In this section, the gain-scheduled nonlinear controller is simulated with nominal values of the missile's aerodynamic coefficients. The scope of these simulations is to demonstrate the fulfillment of the performance specifications, P1 and P2, from Sec. II.B.

In Fig. 12, the reference and the real missile trajectories are shown (η_r and η) for a typical tracking scenario [6]. In Fig. 13a, the tail deflection control signal before and after the actuator (δ_c and δ; thin lines) as well as the nominal control δ_r (thick line) are presented,

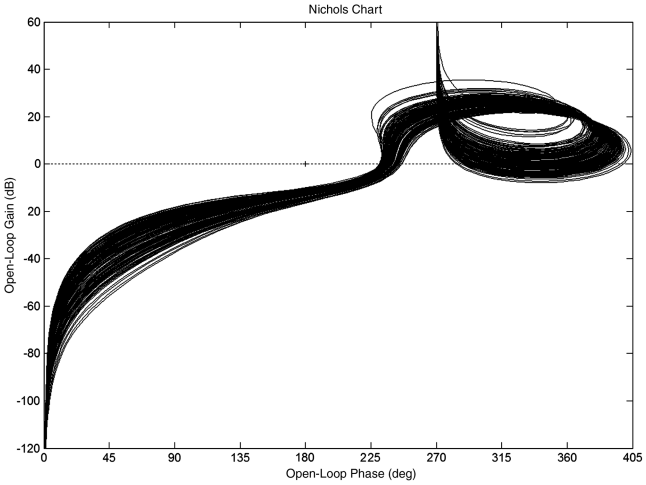

Fig. 11 Nichols chart of the linearized open loops.

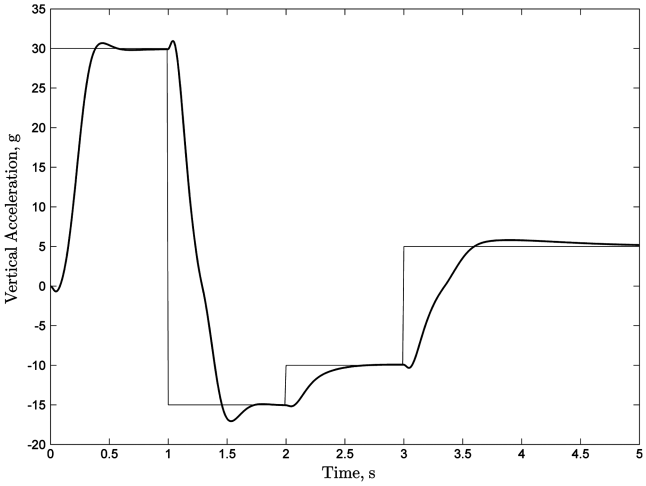

Fig. 12 Reference and real trajectory.

whereas, in Fig. 13b, the tail deflection rate $\dot{\delta}$ is illustrated. It can be seen that the influence of the actuator on the control signal is not noticeable and, in addition, the tail deflection rate is quite small, thus avoiding the overexcitement of the actuator.

Finally, in Table 3, the performance of the autopilot is tabulated (corresponding to P1 and P2 from Sec. II.B) for the four changes of the tracked reference signal η_r, as in Fig. 12. The constraints are well respected while maintaining low rates for the control signal, except

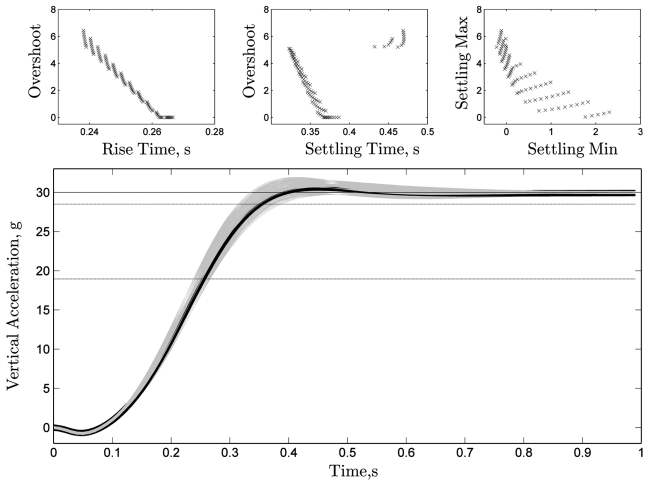

Fig. 10 Feedforward gain optimization.

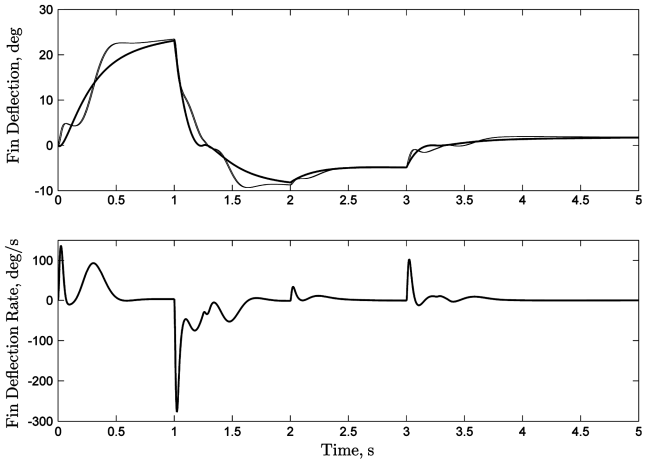

Fig. 13 Control signal and its derivative.

Table 3 Autopilot performance

Point[a]	1	2	3	4
Time constant; τ, s	0.253	0.266	0.246	0.322
Overshoot, %	2.26	5.55	0	5
Steady-state error, %	0.33	0.077	1.5	1.33
Deflection rate [b], deg/s	4.55	6.16	6.72	6.83

[a]This row sorts the four transitions of the reference signal η_r as seen in Fig. 12.
[b]This value corresponds to the normalized (divided by the step amplitude) rate of δ of Fig. 13.

for the steady-state error of points 3 and 4, for which a small violation is observed.

The missile's state is shown in Fig. 14, whereas, in Fig. 15 the gains of the gain-scheduled controller are presented as a function of time. It can be observed that the gains evolve smoothly and no abrupt changes are caused by the changing of operating points. In addition, the gains do not reach a steady state for every operating point, as this is slowly varying due to Mach variation following Eq. (9), thus adapting to this change.

C. Nonlinear Simulations: Perturbed Case

In this section, the robustness of the proposed gain-scheduled controller is tested according to the demands R1 and R2 from Sec. II.B. As far as R1 is concerned, a Monte Carlo analysis of the missile output is run for 150 perturbed combinations of (a_m, b_m, and c_m) and d_m around their nominal values found in Table 1 (see Fig. 16).

In addition, the proposed control scheme's sensitivity to loop gain/delay augmentation is tested. First, the loop gain is changed slowly from 0.75 to 3.2 (corresponding to the 10.1 dB of the gain margin in Sec. VI.A) (see Fig. 17) and, second, the loop delay is changed from 0 to 30 ms (see Fig. 18). The excellent behavior of the controller in the face of the aforementioned uncertainties is observed.

Finally, as far as demand R2 is concerned, the open-loop magnitude frequency response of the family of systems obtained in Sec. VI.A is shown (see Fig. 19). A small of violation of the −30 dB constraint at 300 rad/s is observed; the range of the magnitude frequency response for the linear systems varies from −26 to −34 dB.

In the previous simulations, the nonlinear controller was supposed to be perfectly computed and implemented on the system. The PI/P

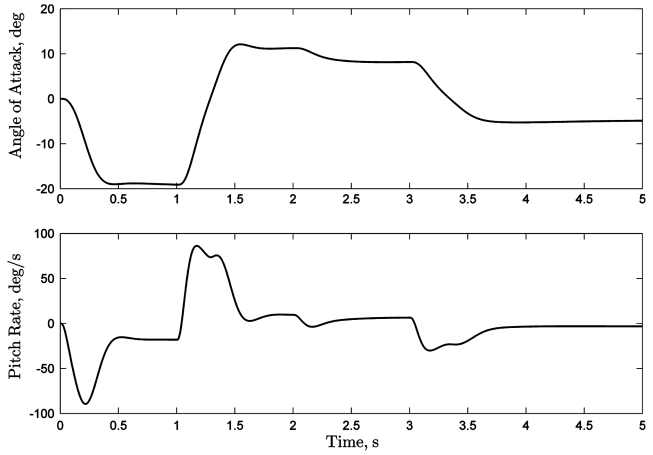

Fig. 14 Missile state.

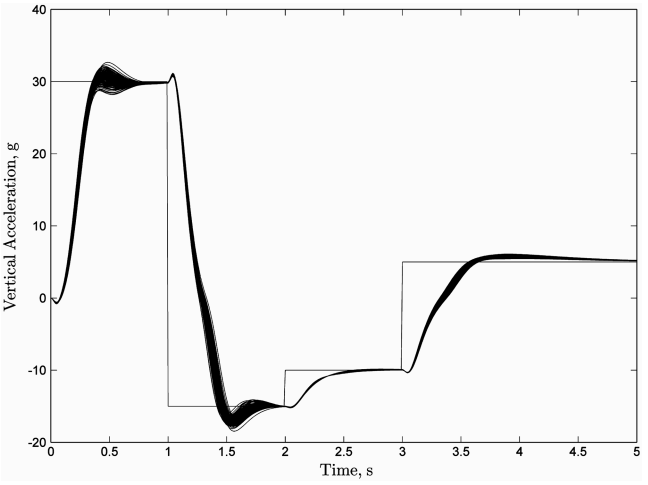

Fig. 16 Parametric robustness of the controller.

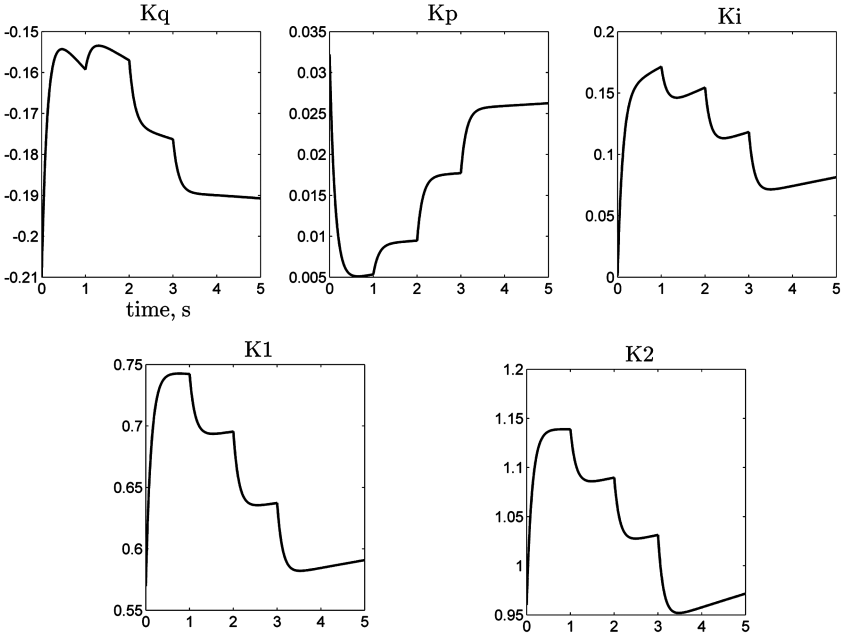

Fig. 15 Controller gains.

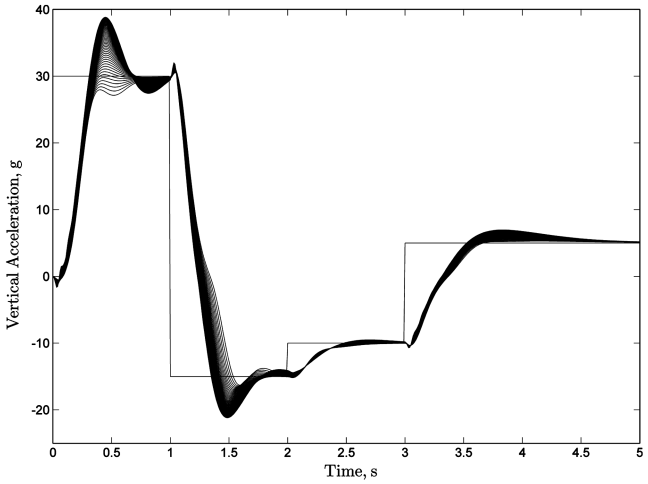

Fig. 17 Loop gain robustness of the controller.

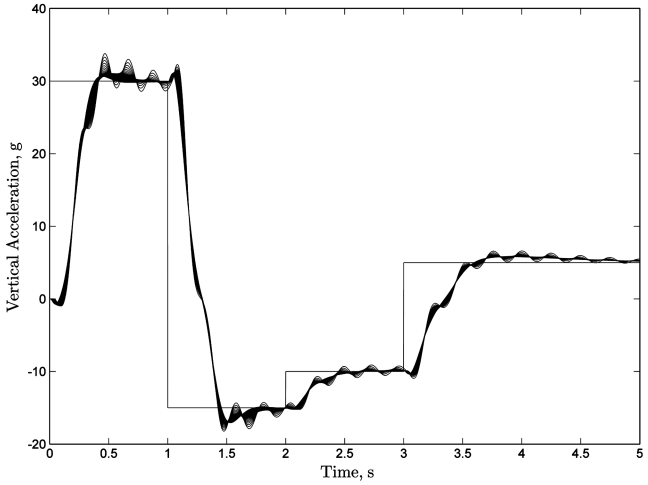

Fig. 18 Loop delay robustness of the controller.

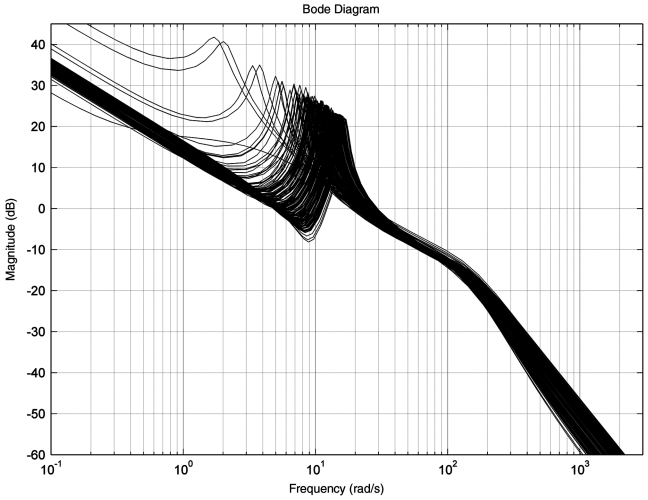

Fig. 19 Frequency response of the linear plants.

filter gains, particularly, are optimized following the procedure in Sec. IV.C at nine operating points, leaving to the $\mathcal{H}_\infty$ controllers the task of robustifying the closed loop. However, in practice, these filters are seldom well adjusted or they are held fixed for a large part of the flight envelope to reduce complexity of the offline controller computation procedure. In the following analysis, the gains K_q, K_p, and K_i are randomly and independently perturbed by 30% around

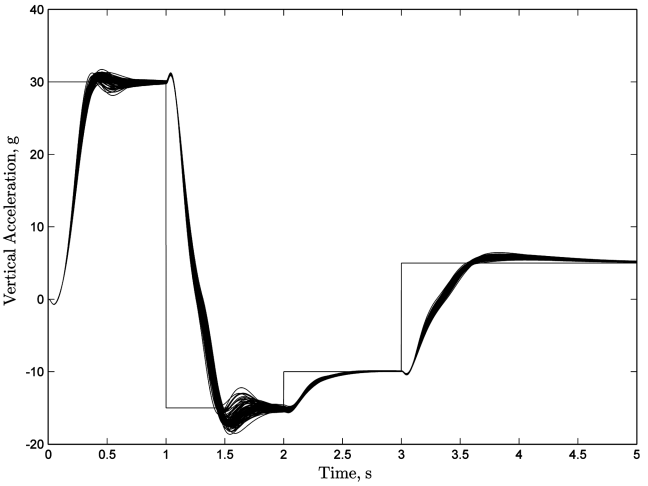

Fig. 20 PI/P controller perturbation.

their nominal values, and the very good behavior of the plant's output is demonstrated (see Fig. 20).

The overall performance of the gain-scheduled control scheme proposed in this paper is clearly superior to the ones proposed in [6,7,9–13], both in terms of performance and/or robustness of the closed loop and in terms of control effort. It does not, however, provide absolute performance with regard to the advantages of this approach, but it does provide simplicity concerning the LTI controllers and the generality with which the autopilot problem is attacked (e.g., operating point selection, interpolation). In addition, in this work, the control scheme proposed has been exhaustively tested with extensive simulations.

VII. Conclusions

In this paper, a novel method for obtaining gain-scheduling controllers for nonlinear-parameter-dependent systems is proposed, offering several enhancements over the existing practice. The goal was threefold and focused on the amelioration of each step of the linearization-based gain-scheduling procedure. The first goal concerns the operating point selection problem; here, an algorithm based on the gap metric is proposed, permitting the avoidance of ad hoc rectangular gridding of the operating domain of the system. The second goal concerns the choice of the simplest possible structure of the linear time invariant controllers used by the gain-scheduling controller for reasons of computational ease and implementability. Static $\mathcal{H}_\infty$ output feedback controllers are used for linear models of the missile shaped by appropriate pre/postfilters of the simplest possible form (proportional and proportional/integral controllers). These robust controllers are, in fact, dictated by the use of the gap metric-based algorithm when choosing the synthesis points of the system. Finally, the third goal was to obtain a method for scheduling the computed controllers that was not redundant, that was easy to calculate, and that would also offer very good results when being used to form the final global nonlinear gain-scheduled controller. This method was based on Delaunay triangulation of the operating domain of the system using the synthesis points calculated by the operating point selection algorithm.

The control scheme considered is applied to a well-known benchmark system, namely, the pitch-axis model of an air–air missile. This system, even though it does not correspond to a real-world one, is very close to the models used in the industry and stays sufficiently globally nonlinear for these types of autopilot controllers to be tested. The problem for the gain-scheduled controller is to properly track vertical acceleration reference signals with a given strict output performance and actuator rate constraints. In addition, several parametric and frequency robustness constraints are imposed and the controller is tested for these and for additional ones concerning heavy loop gain/delay alterations or controller uncertainties.

The method proposed, even though it offers only local stability guaranties for the system, yields the same or better performance and/or robustness than existing design methods but with a simple structure that could be easily implemented on a real-world system. In addition, it remains sufficiently generic for use in other types of systems as its computation procedure remains method oriented and not application oriented. Future work will involve ameliorating the gap metric algorithm using triangular division of the operating domain and testing on a new multi-input/multi-output system.

Acknowledgment

The authors would like to thank the European Aeronautic Defence and Space Company Foundation for the financial support concerning this work.

References

[1] Leith, D. J., and Leithead, W. E., "Survey of Gain-Scheduling Analysis and Design," *International Journal of Control*, Vol. 73, No. 11, 2000, pp. 1001–1025. doi:10.1080/002071700411304

[2] Rugh, W. J., and Shamma, J. S., "Research on Gain Scheduling," *Automatica*, Vol. 36, 2000, pp. 1401–1425. doi:10.1016/S0005-1098(00)00058-3

[3] Apkarian, P., and Biannic, J.-M., "Self-Scheduled H_∞ Control of Missile via Linear Matrix Inequalities," *Journal of Guidance, Control, and Dynamics*, Vol. 18, No. 3, 1995, pp. 532–538. doi:10.2514/3.21419

[4] Stilwell, D. J., and Rugh, W. J., "Interpolation of Observer State Feedback Controllers for Gain Scheduling," *IEEE Transactions on Automatic Control*, Vol. 44, No. 6, 1999, pp. 1225–1229. doi:10.1109/9.769379

[5] Stilwell, D. J., "State-Space Interpolation for a Gain Scheduled Autopilot," *Journal of Guidance, Control, and Dynamics*, Vol. 24, No. 3, 2001, pp. 460–465. doi:10.2514/2.4766

[6] Nichols, R. A., Reichert, R. T., and Rugh, W. J., "Gain Scheduling for H_∞ Controllers: A Flight Control Example," *IEEE Transactions on Control Systems Technology*, Vol. 1, No. 2, 1993, pp. 69–79. doi:10.1109/87.238400

[7] Balas, G. J., and Packard, A. K., "Design of Robust, Time-Varying Controllers for Missile Autopilots," Inst. of Electrical and Electronics Engineers, New York, 1992, pp. 104–110.

[8] Farret, D., Duc, G., and Harcaut, J.-P., "Reduced Order H_∞ Loop-Shaping Control of a Missile Pitch Axis over a Wide Flight Envelope," *International Journal of Nonlinear Studies*, Special Issue on Control in Defense Systems, Vol. 11, No. 2, 2004, pp. 199–214.

[9] Gu, G., Cloutier, J. R., and Kim, G., "Gain Scheduled Missile Autopilot Design Using Observer-Based H_∞ Control," AIAA, Washington, D.C, 1995, pp. 1951–1955.

[10] Lawrence, D. A., Kelly, J. H., and Evers, J. H., "Gain Scheduled Missile Autopilot Design Using a Control Signal Interpolation Technique," AIAA, Reston, VA, 1998, pp. 1394–1402.

[11] Mehrabian, A. R., and Roshanian, J., "Design of Gain-Scheduled Autopilot for a Highly Agile Missile," Inst. of Electrical and Electronics Engineers, New York, 2006, pp. 144–149.

[12] Theodoulis, S., and Duc, G., "Missile Autopilot Design Using Observer-Based Gain Scheduling," International Federation of Automatic Control, Laxenburg, Austria, 2007.

[13] White, D. P., Wozniak, J. G., and Lawrence, D. A., "Missile Autopilot Design Using a Gain Scheduling Technique," Inst. of Electrical and Electronics Engineers, New York, 1994, pp. 606–610.

[14] Zames, G., and El-Sakkary, K., "Unstable Systems and Feedback: The Gap Metric," 1980, pp. 380–385.

[15] Prempain, E., and Postlethwaite, I., "Static H_∞ Loop Shaping Control of a Fly-by-Wire Helicopter," *Automatica*, Vol. 41, Sept. 2005, pp. 1517–1528. doi:10.1016/j.automatica.2005.04.001

[16] McFarlane, D., and Glover, K., "A Loop Shaping Design Procedure Using H_∞ Synthesis," *IEEE Transactions on Automatic Control*, Vol. 37, No. 6, 1992, pp. 759–769. doi:10.1109/9.256330

[17] McFarlane, D., and Glover, K., *Robust Controller Design Using Normalized Coprime Factor Plant Descriptions*, Springer–Verlag, Berlin/New York/Heidelberg, 1990.

[18] Zhou, K., Doyle, J. C., and Glover, K., *Robust and Optimal Control*, Prentice–Hall, Englewood Cliffs, NJ, 1996, Ch. 18.

[19] Georgiou, T. T., and Smith, M. C., "Optimal Robustness in the Gap Metric," *IEEE Transactions on Automatic Control*, Vol. 35, No. 6, 1990, pp. 673–686. doi:10.1109/9.53546